

Laser $^{40}\text{Ar}/^{39}\text{Ar}$ Evaluation of Slow Cooling and Episodic Loss of ^{40}Ar from a Sample of Polymetamorphic Muscovite

W. E. Hames and K. V. Hodges

Volume diffusion models predict that crystals with large diffusion dimensions can record a wide range of thermal conditions in the Earth's crust. Direct measurements of the zoning of radiogenic argon-40 in single muscovite porphyroblasts, from a complex terrain in the Vermont Appalachians, record multiple crustal events that span 150 million years. The crystal radius was the effective dimension for argon diffusion (approximately 1000 micrometers). Late deformation features inside the crystals locally decreased the diffusion dimension and promoted loss of argon-40. Zoning patterns of radiogenic isotopes, as observed in this study, are an increasingly important diagnostic tool for studying the thermal record of tectonic processes.

Orogens typically have extensive regions that experienced superimposed metamorphic events. Polymetamorphic rocks from such regions may record multiple instances of crystallization, reheating, and protracted high-temperature conditions. The $^{40}\text{Ar}/^{39}\text{Ar}$ mineral ages for polymetamorphic rocks are commonly intermediate to the timing of superimposed metamorphisms, recording a relict isotopic component from earlier events, even in cases where the superimposed metamorphism or metamorphisms exceeded the nominal closure temperature of the minerals for a substantial length of time (for muscovite, 1–6). Recent laser studies (4–9) indicate that gradients in ^{40}Ar concentration form at a scale controlled by the crystal size (up to $\sim 1000\ \mu\text{m}$), with a form that is characteristic of the thermal evolution. The occurrence of relict isotopic compositions in thermally complex samples and the scales of isotopic gradients determined by laser studies suggest that grain size, microstructural characteristics, and ionic substitutions have substantial effects on argon retention and closure age. An increased understanding of these controls and selective analytical strategies will permit closure ages to be used in increasingly specific geologic contexts and to obtain age data for geologic time intervals by analysis of single crystals.

In this study we reexamined the distribution of radiogenic ^{40}Ar ($^{40}\text{Ar}^*$) in muscovite crystals from a polymetamorphic rock to test the influence of grain size and microstructure on $^{40}\text{Ar}^*$ diffusion and to evaluate the data by comparison with slow cooling and episodic thermal hypotheses for the study region. The sample is from a landmark study by Lanphere and Albee (1), which was one of the first to show that texturally different generations of a mineral

in a polymetamorphic rock can yield different $^{40}\text{Ar}/^{39}\text{Ar}$ ages.

Sample LA384A (1) contains primary muscovite porphyroblasts (up to 4 mm in diameter and 1 mm thick), secondary chlorite (commonly as pseudomorphs after garnet), and aggregates of secondary, finely grained white mica (commonly pseudomorph after kyanite). The muscovite porphyroblasts display limited intracrystalline strain features (some undulose extinction and kink bands), and the rock was not pervasively deformed after porphyroblast development. Sample LA384A yielded $^{40}\text{Ar}/^{39}\text{Ar}$ incremental-heating plateau and isochron ages of 420 ± 9 and 422 ± 3 Ma (million years ago), respectively (1). The data seemed to reflect a homogeneous distribution of $^{40}\text{Ar}^*$, which resulted from only in situ decay of ^{40}K after Ordovician metamorphism, and to indicate no appreciable loss of accumulated $^{40}\text{Ar}^*$ during the superimposed event. White mica pseudomorphs after kyanite from the same sample yielded plateau and isochron ages of 343 Ma, which was interpreted as a minimum estimate for the timing of the superimposed event (1).

Although the initial data for the primary muscovite seem straightforward, some characteristics of the release spectrum (1) suggest that $^{40}\text{Ar}^*$ is distributed inhomogeneously: the first increment yielded an age of 405 Ma, subsequent increments generally increased in age, and the final increment gave an age of 435 Ma. These data can be interpreted to indicate that the sample has been disturbed and that a naturally varying isotopic distribution was partly homogenized during the analysis.

The new data (10) define a broadly concentric age distribution with regions of decreased age inside the crystal (Fig. 1). Maximum ages are 462 Ma (in the core of the sample), and ages generally decrease toward the edges of the crystal prism. Ages

along the edge vary from about 420 to 440 Ma. Electron microprobe analyses (of the same 001 cleavage surface represented in Fig. 1) indicate that the sample is not zoned with respect to its major element composition. This is also evident isotopically, as there is no systematic variation in apparent K/Ca or K/Cl ratios in the crystal; moreover, the concentrations of atmospheric argon in the extracted gas (typically less than 5%) do not vary spatially or with age.

Two prominent regions in the crystal yielded ages younger than 420 Ma and seem anomalous with respect to the overall pattern. Spot-fusion ages of 413 to 419 Ma form one linear trend, and a second group of ages, ranging from 404 to 429 Ma, occurs in a linear trend oriented 120° from the first. The first group of ages coincides with the trace of well-defined 010 cleavage planes on 001, and the three analyses of the second group are each centered on $1\bar{1}0$ cleavage (Fig. 1). An age of 432 Ma was obtained inside the crystal in a region of intersecting 010 and $1\bar{1}0$ cleavage. The most abrupt age gradients, and the youngest ages, are near these internal cleavage planes: for instance, 460 to 404 Ma over about $200\ \mu\text{m}$ near the $1\bar{1}0$ cleavage plane (Fig. 1B). Regions of the crystal characterized by the broad age gradients were free from prominent 010 and $1\bar{1}0$ cleavage. Cleavages evident on the 001 plane of this sample appear to represent intercrystalline deformation features formed on 010 and $1\bar{1}0$.

We believe that the apparent age pattern of Fig. 1 is not substantially affected by extraneous, unsupported ^{40}Ar for two reasons: (i) extraneous ^{40}Ar would concentrate in the rims of a porphyroblast and favor radially increasing age (8) and (ii) we have found that the small amounts of ^{36}Ar in the sample seem correlated with an atmospheric source that has a modern $^{40}\text{Ar}/^{36}\text{Ar}$ ratio. Inasmuch as sample LA384A does not have any observable variation in major element chemistry, the decreases in apparent age toward the rims and cracks correspond to decreases in the concentration of $^{40}\text{Ar}^*$ and the $^{40}\text{Ar}^*/\text{K}$ ratio.

"Ages for the peak Taconian metamorphism in Vermont generally are 460 ± 10 Ma" (11, p. 398) and magnesio-hornblende from northern Vermont yielded a $^{40}\text{Ar}/^{39}\text{Ar}$ isochron age of 460 ± 6 Ma (11). The $^{40}\text{Ar}/^{39}\text{Ar}$ ages for the Acadian metamorphism in the region are generally between 375 and 390 Ma (11–15). Metamorphic ages between 460 and 410 Ma in western New England are generally interpreted as recording protracted cooling after Middle Ordovician metamorphism (12, 13, 15). We accept 390 Ma as a maximum estimate for the timing of peak Acadian metamorphism; however, the Late Ordovician to Early Devonian thermal evolution of north-

Department of Earth, Atmospheric, and Planetary Sciences, Massachusetts Institute of Technology, Cambridge, MA 02139.

ern Vermont is not well constrained at present.

The regional constraints available suggest that the concentric gradient in sample LA384A did not form during Devonian metamorphism (as minimum rim ages are about 420 Ma) and that it could have formed during protracted cooling from 460 to 420 Ma, during an episodic loss event after 460 Ma, or as part of a complex combination of both. In addition, a varying distribution of crystallographic defects could affect diffusion gradients, and the map in Fig. 1 indicates that defects are at least locally important. We can use diffusion models (16–18) and the limited data for muscovite diffusion characteristics (19) to further evaluate these alternative hypotheses and the characteristics of diffusion processes that may have formed the gradients.

During an episodic event the fraction of a chemical species lost from a mineral with a cylindrical geometry is given by (16, 20)

$$f = (t_a - t_i) / (t_e - t_i) = 1 - 2/a \cdot \sum [\exp(-D\alpha_n^2 t) J_0(\alpha_n r)] / [\alpha_n J_1(\alpha_n a)] \quad (1)$$

Concentration profiles are lines of constant Dt/a^2 in plots of f versus r/a (16). The total fraction of a chemical species lost from a mineral corresponds to a specific value of Dt/a^2 , and thus we can predict the form of the concentration profile from the fraction of loss for the whole crystal. The average age of the crystal in Fig. 1 is 444 Ma (obtained by cutting the figure along age contours and weighing the pieces). If the loss is due solely to an episodic event at 390 Ma, then $f = 0.26$ and $Dt/a^2 = 0.015$ for the whole crystal; similarly, for an event at 420 Ma, $f = 0.43$ and $Dt/a^2 = 0.045$.

During slow cooling the diffusion coefficient decreases exponentially with temperature, and thus Eq. 1 must be modified (18, 20). The closure temperature (T_c) distribution in a mineral that cooled at a slow, constant rate (from no retention to complete retention) is defined by

$$E/RT_c = G(x) + \ln(TD_0/a^2) \quad (2)$$

We used Eq. 2, the cylinder-model diffusion data for muscovite (19), and $a = 1000 \mu\text{m}$ to calculate that the core of sample LA384A would have closed at 665 K and the rim at 526 K, with an average cooling rate over the interval from 462 to 420 Ma of 3.3 K/Ma; we then used this average cooling rate and Eq. 2 to predict a model age profile for the crystal.

The analyses that define the concentric gradient typically have a higher fractional loss for a given fractional radius than predicted for an event at 390 Ma (Fig. 2A). The episodic loss model at $t_e = 390$ Ma predicts that the outer 100 μm of the sample ($r/a > 0.9$) would have experienced

greater than 60% gas loss, thus suggesting ages of roughly 400 Ma for 100- μm -diameter spot-fusion extraction analyses along the sample edge. Thus, the concentric gradient we have observed does not appear to conform with the simple episodic loss model at 390 Ma. Note also that $^{40}\text{Ar}^*$ loss from areas near cleavage does not appear con-

trolled by the physical grain size (Fig. 1), and $^{40}\text{Ar}^*$ loss is enhanced in these areas relative to fractional radius (Fig. 2A). Thus, the scale, and perhaps the mechanism, of $^{40}\text{Ar}^*$ loss along the cleavage was very different from that which controlled the concentric gradient.

The slow cooling model predicts an ex-

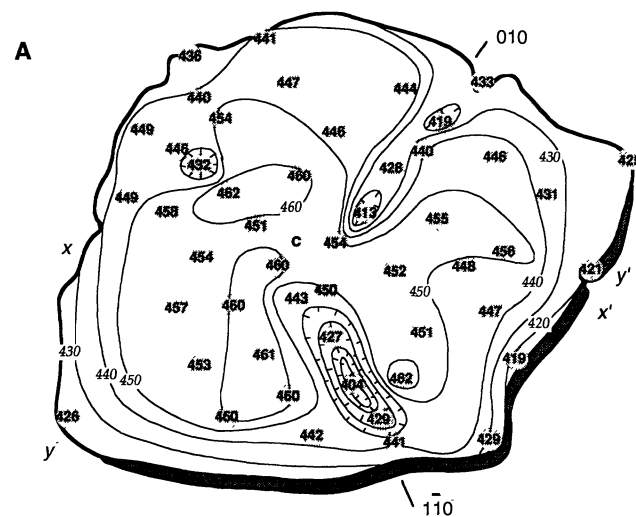


Fig. 1. Age contour map and profiles for the muscovite porphyroblast from sample LA384A. The scale is indicated in (B), the contour interval is 10 million years, and labels have units in Ma. Round, shaded regions in (A) indicate the positions of spot-fusion analyses used to construct the contours. The crystallographic orientation of prominent cleavages is indicated, as is the presumed center of the crystal (c). Two patches of chlorite were evident within the 001 cleavage of the sample [near y in (A)] and were avoided during analysis. The presumed timing for the main porphyroblast development of the Taconian and Acadian metamorphisms (Tm1 and Tm2, respectively) are indicated in (B). Solid symbols on the age profiles represent spot-fusion analyses and their 2σ errors, and open symbols represent intersections with age contours.

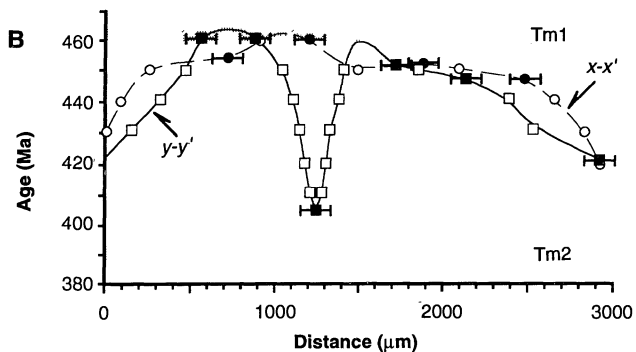


Fig. 2. The relations between fractional change in age (f) and fractional radius (r/a) for all the data of Fig. 1. The error in determining f is roughly the size of the symbol, and the error in r/a is qualitatively estimated at $\pm 10\%$. The effective diffusion dimension (a) for model calculations is 1000 μm , and $r/a = 0$ at point c in Fig. 1A; t_e is the time of an episodic gas loss event in the calculations and t_{c-rim} is the timing of closure of the rim for the slow cooling model. Analyses near internal cleavage are represented in (A) by solid squares, and those that define the concentric gradient are represented by open circles. (A) Model concentration profile for episodic loss at 390 Ma. (B) Model profiles for episodic loss (t_e) and closure upon cooling (t_{c-rim}) at 420 Ma.

ponentially decreasing concentration with fractional distance (Fig. 2B). The data define a linear decrease in concentration (21), for fractional distances greater than about 0.5, which is compatible with the episodic loss model for an event at 420 Ma (Fig. 2B).

A comparison of the data with diffusion models indicates that loss of ⁴⁰Ar in sample LA384A occurred by way of cylindrical volume diffusion, over a scale of 1000 μm, between about 460 and 420 Ma. Our preferred interpretation is that after retention of ⁴⁰Ar* in the core of the crystal at 462 Ma, close to the timing of peak metamorphism, lower greenschist grade retrogression at 420 Ma formed the isotopic gradient. The sample did not experience substantial volume diffusion loss of ⁴⁰Ar* after 420 Ma; however, ⁴⁰Ar* was lost from areas inside the crystal that were deformed in Early Devonian time.

REFERENCES AND NOTES

1. M. A. Lanphere and A. L. Albee, *Am. J. Sci.* 274, 545 (1974). We have recalculated all ages using the decay constants of R. H. Steiger and E. Jäger [*Earth Planet. Sci. Lett.* 36, 359 (1977)].
2. C. Chopin and H. Maluski, *Contrib. Mineral. Petrol.* 74, 109 (1980).
3. J. R. Wijbrauns and I. McDougall, *ibid.* 93, 187 (1989).
4. S. Scaillet, G. Feraud, Y. Lagabrielle, M. Balleuvre, G. Ruffet, *Geology* 18, 741 (1990).
5. S. Scaillet, G. Feraud, M. Balleuvre, M. Amouric, *Geochim. Cosmochim. Acta* 56, 2851 (1992).
6. K. de Jong, J. R. Wijbrauns, G. Feraud, *Earth Planet. Sci. Lett.* 110, 173 (1992).
7. D. Phillips and T. C. Onstott, *Geology* 16, 542 (1988).
8. J. K. W. Lee, T. C. Onstott, J. A. Hanes, *Contrib. Mineral. Petrol.* 105, 87 (1990).
9. S. P. Kelley and G. Turner, *Earth Planet. Sci. Lett.* 107, 643 (1991).
10. Micras were hand-picked from the center of quartz lens LA384A after crushing and were irradiated in the core of the Los Alamos National Laboratory reactor ($J = 0.01070 \pm 0.00005$). The neutron fluence was monitored with MMhb-1 [S. D. Sampson and E. C. Alexander, *Chem. Geol.* 66, 27 (1987)], and reactions on K and Cl were also monitored with K₂SO₄ and KCl in the irradiation package. Crystals were cleaved into three sections on 001 with a scalpel, and a central section (200 μm thick) was analyzed with a MAP 215-50 mass spectrometer (sensitivity = 2.7×10^{-4} A/torr at an accelerating voltage of 3 kV, multiplier gain = 10,000). The signal evolution was linear during the analysis. Heating with a 10-W Coherent Ar-ion laser (0.25 to 1.0 s with a beam 25 μm in diameter) produced hemispherical melt pits 50 to 100 μm in diameter in the mica; melt pits were surrounded by a dehydration zone, and the overall diameter of the melting and dehydration region was roughly 150 μm. The size of the laser extraction pit was controlled to yield samples for which ⁴⁰Ar and ³⁹Ar were 50 to 300 times greater than the blank. An operational blank was analyzed after every five analyses in the present study, and nominal operational blanks were as follows: ⁴⁰Ar, 6×10^{-16} mol; ³⁹Ar, 1×10^{-17} mol; ³⁸Ar, 2×10^{-18} mol; ³⁷Ar, 1×10^{-17} mol; and ³⁶Ar, 5×10^{-18} mol. Radiogenic yields from the laser analyses were consistently greater than 85% and typically exceeded 95%. The precision of ⁴⁰Ar and ³⁹Ar measurements was generally about 0.5%, and the total error (combined J-value accuracy and sample precision) for ages was about ±1%.

11. J. Laird, M. A. Lanphere, A. L. Albee, *Am. J. Sci.* 284, 376 (1984).
12. J. F. Sutter, N. M. Ratcliffe, S. B. Mukasa, *Geol. Soc. Am. Bull.* 96, 123 (1985).
13. W. E. Hames, R. J. Tracy, N. M. Ratcliffe, J. F. Sutter, *Am. J. Sci.* 291, 887 (1991).
14. F. M. Hueber, W. A. Bothner, N. L. Hatch, S. C. Finney, J. N. Aleinikoff, *ibid.* 290, 360 (1990).
15. F. S. Spear and T. M. Harrison, *Geology* 17, 181 (1989).
16. J. Crank, *The Mathematics of Diffusion* (Oxford Univ. Press, New York, ed. 2, 1975).
17. M. H. Dodson, *Contrib. Mineral. Petrol.* 40, 259 (1973).
18. ———, *Mater. Sci. Forum* 7, 145 (1986).
19. G. A. Robbins, thesis, Brown University (1972).
20. We substitute apparent age for concentration of ⁴⁰Ar* in Eq. 1. Additional symbols for Eqs. 1 and 2 are as follows: t_a is apparent age, t_i is 462 Ma (the oldest ages from the core of the sample), t_e is the timing of the event of interest (either 420 or

390 Ma), a is the diffusion dimension, r is the radial distance, D is the diffusion coefficient, E is activation energy, t is the temperature of the loss event, α_n represents roots of the Bessel functions $J_0(x)$ and $J_1(x)$, R is the gas constant, and $G(x)$ and T are functions with tabulated values (18).

21. Although ages on the rims of the crystal vary from 440 to 420 Ma (Fig. 1), they are systematic with respect to distance from the presumed center of the crystal (Fig. 2B). We interpret that the distance from point c in Fig. 1 to the perimeter of the original crystal was a roughly uniform 1000 μm, and ages of about 430 to 440 Ma presently occur along edges broken during sample preparation.
22. We thank A. Albee for providing the samples for this study. This manuscript was improved by thoughtful reviews from G. B. Dalrymple and T. C. Onstott and discussions with R. J. Cumbest and W. J. Olszewski.

16 April 1993; accepted 26 July 1993

Activation of Floral Homeotic Genes in *Arabidopsis*

Detlef Weigel* and Elliot M. Meyerowitz†

The identity of floral organs in *Arabidopsis thaliana* is determined by homeotic genes, which are expressed in specific regions of the developing flower. The initial activation of homeotic genes is accomplished at least in part by the products of two earlier acting genes with overlapping functions. These are the floral meristem-identity genes *LEAFY* and *APETALA1*. The requirements of *LEAFY* and *APETALA1* activity vary for different homeotic genes.

Flowers of *Arabidopsis* are composed of four types of organs: sepals, petals, stamens, and carpels. The floral organs are arranged in concentric rings, or whorls. Sepals occupy the first, outermost whorl, petals the second whorl, stamens the third whorl, and carpels, which form the central gynoecium, the fourth, central whorl. Organ identity in the flower is determined by three classes of homeotic genes, A, B, and C, each of which acts in two adjacent whorls. In this way, every whorl has a distinct combination of homeotic functions: class A alone in the first whorl, classes A and B in the second whorl, classes B and C in the third whorl, and class C alone in the fourth whorl (1). In all cases in which the RNA expression pattern has been reported, RNA of a homeotic gene accumulates in those whorls of the wild-type flower where the gene is active, as deduced from its mutant phenotype (2–6).

The region-specific expression of homeotic genes is brought about mainly by negative interactions. For example, the expression of the class C gene *AGAMOUS* (*AG*) is repressed in the outer whorls by the class A gene *APETALA2* (*AP2*) (1, 3), and the expression of the

class B genes *APETALA3* (*AP3*) and *PISTILLATA* (*PI*) is repressed in the central whorl by the whorl-identity gene *SUPERMAN* (6–8). However, little is known about the initial activation of homeotic genes, probably accomplished by positive regulators. The candidates for such activators are two genes, *LEAFY* (*LFY*) and *APETALA1* (*AP1*), that control floral meristem identity and whose inactivation causes the partial transformation of flowers into shoots (9–13). The determination of floral meristem identity precedes that of floral organ identity, and consistent with this early function, the expression of *LFY* and *AP1* is initiated earlier than that of the homeotic genes (5, 11). To understand better the effect of *LFY* and *AP1* on homeotic gene activity, we analyzed how *lfy* and *ap1* mutations affect the expression of homeotic genes that determine floral organ identity.

The two B function genes *AP3* and *PI* are expressed in the developing second and third whorls, which give rise to petals and stamens (4, 6) (Figs. 1A and 2A). Second- and third-whorl organs are affected differently by *ap1-1* and *lfy-6* mutations, both of which are apparently complete loss-of-function alleles (14). In *ap1-1* mutants, the stamens of the third whorl are normal, but second-whorl organs typically fail to develop (9, 13). In *lfy-6* mutant flowers, none of the inner

California Institute of Technology, Division of Biology 156-29, Pasadena, CA 91125.

*Present address: Department of Biology 0116, University of California, San Diego, La Jolla, CA 92093.
†To whom correspondence should be addressed.